

Measurements of the Aeroacoustic Sound Source in Hot Jets

James Bridges and Mark Wernet
Glenn Research Center, Cleveland, Ohio

The NASA STI Program Office . . . in Profile

Since its founding, NASA has been dedicated to the advancement of aeronautics and space science. The NASA Scientific and Technical Information (STI) Program Office plays a key part in helping NASA maintain this important role.

The NASA STI Program Office is operated by Langley Research Center, the Lead Center for NASA's scientific and technical information. The NASA STI Program Office provides access to the NASA STI Database, the largest collection of aeronautical and space science STI in the world. The Program Office is also NASA's institutional mechanism for disseminating the results of its research and development activities. These results are published by NASA in the NASA STI Report Series, which includes the following report types:

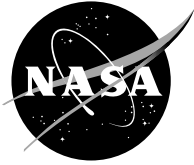
- **TECHNICAL PUBLICATION.** Reports of completed research or a major significant phase of research that present the results of NASA programs and include extensive data or theoretical analysis. Includes compilations of significant scientific and technical data and information deemed to be of continuing reference value. NASA's counterpart of peer-reviewed formal professional papers but has less stringent limitations on manuscript length and extent of graphic presentations.
- **TECHNICAL MEMORANDUM.** Scientific and technical findings that are preliminary or of specialized interest, e.g., quick release reports, working papers, and bibliographies that contain minimal annotation. Does not contain extensive analysis.
- **CONTRACTOR REPORT.** Scientific and technical findings by NASA-sponsored contractors and grantees.

- **CONFERENCE PUBLICATION.** Collected papers from scientific and technical conferences, symposia, seminars, or other meetings sponsored or cosponsored by NASA.
- **SPECIAL PUBLICATION.** Scientific, technical, or historical information from NASA programs, projects, and missions, often concerned with subjects having substantial public interest.
- **TECHNICAL TRANSLATION.** English-language translations of foreign scientific and technical material pertinent to NASA's mission.

Specialized services that complement the STI Program Office's diverse offerings include creating custom thesauri, building customized databases, organizing and publishing research results . . . even providing videos.

For more information about the NASA STI Program Office, see the following:

- Access the NASA STI Program Home Page at <http://www.sti.nasa.gov>
- E-mail your question via the Internet to help@sti.nasa.gov
- Fax your question to the NASA Access Help Desk at 301-621-0134
- Telephone the NASA Access Help Desk at 301-621-0390
- Write to:
NASA Access Help Desk
NASA Center for Aerospace Information
7121 Standard Drive
Hanover, MD 21076



Measurements of the Aeroacoustic Sound Source in Hot Jets

James Bridges and Mark Wernet
Glenn Research Center, Cleveland, Ohio

Prepared for the
Ninth Aeroacoustics Conference and Exhibit
cosponsored by the American Institute of Aeronautics and Astronautics
and the Confederation of European Aerospace Societies
Hilton Head, South Carolina, May 12–14, 2003

National Aeronautics and
Space Administration

Glenn Research Center

Acknowledgments

We thank the program manager of NASA's Quiet Aircraft Technology program, Joe Grady, and the Glenn Research Center Acoustic Branch management for support of this work. We thank Trevor John and Gary Clayo for their skillful assistance in putting together the optical/mechanical marvel that allowed these measurements to be made.

Available from

NASA Center for Aerospace Information
7121 Standard Drive
Hanover, MD 21076

National Technical Information Service
5285 Port Royal Road
Springfield, VA 22100

Available electronically at <http://gltrs.grc.nasa.gov>

MEASUREMENTS OF THE AEROACOUSTIC SOUND SOURCE IN HOT JETS

James Bridges and Mark Wernet
National Aeronautics and Space Administration
Glenn Research Center
Cleveland, Ohio 44135

Abstract

We have succeeded in measuring a substantial portion of the two-point space-time velocity correlation in hot, high-speed turbulent jets. This measurement, crucial in aeroacoustic theory and the prediction of jet noise, has been sought for a long time, but has not been made due to the limitations of anemometry. Particle Image Velocimetry has reached a stage of maturity where sufficient measurement density in both time and space allow the computation of space-time correlations. This paper documents these measurements along with lower-order statistics to document the adherence of the jet rig and instrumentation to conventional measures of the turbulence of jets. These measures have been made for a simple round convergent nozzle at acoustic Mach numbers of 0.5, 0.9, both cold and at a static temperature ratio of 2.7, allowing some estimation of the changes in turbulence that take place with changes in jet temperature.

Since the dataset described in this paper is very extensive, attention will be focused on validation of the rig and of the measurement systems, and on some of the interesting observations made from studying the statistics, especially as they relate to jet noise. Of note is the effort to study the acoustically relevant part of the space-time correlation by addressing that part of the turbulence kinetic energy that has sonic phase speed.

MOTIVATION

Aeroacoustic questions

Acoustic analogy and source description

As has often been noted, jet noise theory ultimately relies on a knowledge of turbulent flow statistics that has been beyond our capability to measure and possibly beyond any practical ability to measure accurately enough. The fourth-order two-point space-time correlation that lies at the heart of conventional acoustic analogies is a daunting quantity to measure, especially in a hot high-speed jet. In their 2002 AIAA/CAES Aeroacoustics Meeting paper, Seiner et al.¹ summarized the need for two-point space-time correlations in aeroacoustic research. They gave expressions for the source terms of the acoustic analogy formulation in terms of these correlations and discussed methods by which such measurements might be obtained.

Historically, jet noise predictions based upon the acoustic analogy, whether motivated by Lighthill's² formulation or by Lilley's³, all derived their models of these source terms from a combination of simple theoretical considerations and very limited experimental results. Theoretically, the work of Batchelor⁴, using assumptions of isotropy and homogeneity, often played a big part in formulating models. Experimentally, the work of Chu⁵ is often cited to support the chosen functional forms employed. These are *prima facie* rather poor support because turbulence

in a jet is neither isotropic nor homogeneous, and Chu's remarkable data only covers the first few jet diameters of an extremely low speed ($M_j=0.3$), cold jet.

Previous data sources

Besides the work of Chu, several fine studies on jet turbulence have been reported. Laurence⁶ measured two-point, two component spatial correlations and spectra in a moderate Mach number cold jet using early hot-wire techniques. Davies et al.⁷ also made space-time measurements of cold, low-speed jets, deriving length and timescales from their measurements. Bradshaw et al.⁸ expanded the scope, documenting the spatial correlations for all six independent components of the correlation matrix with three-dimensional displacements. Moving up to heated jets, the LDV measurements of Lepicovsky contained in⁹ provide valuable single-point turbulence measurements in hot subsonic jets.

More recently, several papers have shown the general feasibility of using modern optical methods to measure the space-time velocity correlations in a jet (Oakley et al.¹⁰, Hu et al.¹¹). However, given the extreme sensitivity of the acoustic analogy to the accuracy of the input source terms, it is not clear how these correlations can be used in acoustic analogy formulations. Indeed, it is not certain that experimental measurements of any kind will be accurate enough to capture the acoustically significant details of the source terms!

Previous models

Several physics-based jet noise prediction codes^{12, 13, 14} use models for the space-time correlation of turbulent velocity fluctuations to compute the sound generated by a jet flow from a knowledge of the single-point turbulence statistics. These methods achieve a reasonable degree of success for observer angles near normal to the jet axis; they uniformly fail to predict the observed change in jet noise as the observer moves near the jet axis. It has been noted by Hunter¹⁵ that this change, primarily consisting of a change in peak frequency, can be obtained by changing the scaling of the turbulence model as the observer angle approaches the jet axis. However, there is no experimental support for this being a feature of the modeled two-point correlation. Hopefully by examining actual two-point space-time velocity correlations a shortcoming in the current, commonly used models will be discovered which will improve the state of jet noise prediction. Likewise, it is hoped that several long-standing questions concerning the behavior of the source terms with changes in jet temperature and location within the plume can be resolved with the measurements. Among the issues to be resolved are the validity of the approximation of the fourth order correlation by products of second order correlations, the proper form for the correlation model in space and time, and the question of whether there is any feature in the source terms that would cause an apparent change in the character of the source with observer angle.

Present work

Before computing high-order, multi-dimensional statistics from the data, low-order measurements made with the dual PIV system were evaluated against low Mach number, cold hotwire data and other historical data to determine their validity. Single-point statistics, such as mean velocity, turbulent kinetic energy, and turbulence anisotropy have been computed from the measurements, and the effect of Mach number and temperature quantified. The two-point correlations have been analyzed in part by comparing them with common models for the space-time correlation.

The current paper seeks to present the methods used to obtain the data and the efforts made to determine its validity. In-depth analysis is still to be made on the high-order statistics, including Fourier space representations of the data.

NOMENCLATURE

One-point statistics

Following standard turbulence nomenclature, subdivide the instantaneous velocity vector \vec{U} into time mean $\overline{U}_i(\vec{x})$ and fluctuating $\overline{u_i^2}$ parts. In this study,

measurements were taken in the axial (x_1) and radial (x_2) planes and only the axial and radial components of velocity were measured. For comparisons with Reynolds-averaged Navier-Stokes solutions, turbulence is assumed to be axisymmetric about the direction of the mean flow and the turbulent kinetic energy is defined as

$$TKE = \frac{1}{2} \left(\overline{u_1^2} + \overline{u_2^2} + \overline{u_3^2} \right),$$

Two-point statistics

Our interest in two-point statistics is driven by aeroacoustic theory. Specifically, most aeroacoustic theory requires knowledge of two-point space-time correlations of the velocity field:

$$\mathbf{R}_{ij}(\vec{\xi}, \tau, \vec{x}) = \overline{u_i'(\vec{x} + \vec{\xi}/2, t) u_j'(\vec{x} - \vec{\xi}/2, t + \tau)} = \overline{u_i' u_j'}$$

where the prime on u_j indicates that the velocity is taken at a point different from u_i by a small displacement $\vec{\xi}$ and a time delay τ about the spatial point \vec{x} . $\mathbf{R}(\vec{\xi}, \vec{x})$ has five terms (assuming symmetry) in three spatial dimensions for every point in physical space. Further, since we only have two components of velocity in a plane, we only can compute three of the five components in two dimensions in a plane.

The correlation is normalized in our data by the reference variances,

$$R_{ij}(\vec{\xi}, \tau, \vec{x}) = \overline{u_i' u_j'} / \sqrt{\overline{u_i^2} \overline{u_j^2}}.$$

Integral length and timescales are computed in various directions using the following nomenclature:

$$L_{ij}(\vec{x}) = \frac{1}{2} \int_{-\infty}^{\infty} \mathbf{R}_{ii}(\xi_j, \tau, \vec{x}) d\xi_j$$

$$T_i(\vec{x}) = \frac{1}{2} \int_{-\infty}^{\infty} \mathbf{R}_{ii}(\xi_{peak}, \tau, \vec{x}) d\tau$$

FACILITY

SHJAR

The Small Hot Jet Acoustic Rig (SHJAR) is a single-stream hot jet rig that can cover the range of Mach numbers up to Mach 2, and static temperature ratios up to 2.8 using a hydrogen combustor and central air compressor facilities. For most testing SHJAR uses a 50mm diameter nozzle, but can operate larger nozzles with some limitation on cold setpoints at high Mach number. The SHJAR is located within the AeroAcoustic Propulsion Laboratory (AAPL) at NASA's John H. Glenn Research Center. The AAPL is a 65 foot radius geodesic dome with its interior covered by sound absorbent wedges that provide the anechoic

environment required to study propulsion noise from the several rigs that are located within. The jet rigs are positioned such that they exhaust out the open doorway, allowing the flows to be seeded and removing issues related to background noise from flow collectors.

The nozzle being used in this test is one of a family of convergent nozzles, called the Acoustic Reference Nozzles (ARN), designed to be simple to characterize with similar dimensions such as inlet diameter (15.24mm), lip thickness (1.27mm), outside face angle (30° to jet axis), and parallel flow section at the exit (6.4mm). Along with a 0.5m long settling chamber and thermocouple/pitot-static tube, this nozzle system is shared between NASA jet facilities and is envisioned as a reference for other jet noise facilities (Figure 1). The settling chamber contains a series of screens located 18" upstream of the nozzle entrance to isolate the jet initial condition from small vagaries of the jet rig such as boundary layers. For this test, the ARN2, a 50.1mm or 2" nozzle, was used.

INSTRUMENTATION

PIV components

Two PIV systems were used for this experimental effort, tied together via a triggering circuit with variable time delay. Each PIV system consisted of a dual head Nd:YAG laser operating at 532 nm generating a 400 mJ/pulse light sheet containing the jet axis. Each laser was coordinated with a single 2000 by 2000 pixel dual-frame camera viewing the light sheet at right angles, one on each side of the light sheet. Image frame pairs were obtained by straddling adjacent frame boundaries. A PCI frame digitizer was used to acquire image data directly to disk in 200 image-pair sequences. Each camera viewed the same 170mm square field of view, centered on the jet axis, from a distance of 1.4m. Figure 2 shows the optical layer relative to the jet rig. Because the AAPL is open to the outdoors and could not be run in total darkness, optical backgrounds for the cameras had to be provided. The cameras each peered through aluminum plates covered in black velvet, providing a dark uniform background for each other. These are not shown in the figure for clarity.

Both PIV systems were mounted on a large axial traverse that carried all power supplies, laser heads, cameras, and acquisition computers. This traverse had a range of roughly 2.5m with an accuracy of 1mm. One of the PIV systems was further mounted on a secondary axial traverse atop the primary traverse, giving it a displacement relative to the primary, or fixed, PIV system. The laser head and optics were mounted on one high-precision positioner while the associated camera was mounted on a synchronized positioner. The

secondary traverse had a range of 1m with an accuracy of 0.01mm. Alignment of the two PIV systems was accomplished by registering both camera images on a two-sided optical target in the plane of the light sheet and by registering of the light sheets on a fixed target using light sensitive paper, paying special attention to the edges of the light sheet image.

Key to the success of the effort was the use of cross-polarization of the laser beams and polarizers on the PIV cameras. The first PIV system was configured to use 'p'-polarized light and its camera was equipped with a polarizer to only pass 'p' polarized light. The second PIV system was configured to use 's'-polarized light while its camera only sensed 's'-polarized light. Without this polarization, light from the second PIV system laser became a 'noise' to the first system's second image, raising the signal to noise ratio of the image cross-correlation to an unacceptable level. Polarization reduced the image intensity of the second system on the first system to a level which allowed successful cross-correlation for both systems.

Velocity maps were computed from the image pairs using conventional multipass PIV algorithms with error detection based upon image correlation signal to noise ratio (NASA PIVPROC software). All datasets used had a data quality metric of 0.9 or better, where data quality is defined as the number of accepted velocity vectors at a location relative to the total number of image pairs acquired. Final velocity maps had a spatial resolution of 0.02D_j. A minimal number of velocity maps (200) were acquired at each space-time separation to obtain rough estimates of the correlations. Based upon convergence of the statistics, the error in the final correlation data is estimated at ±5%.

Seeding

As alluded to by Seiner et al.¹, providing uniform seeding in a jet flow is essential and difficult. This is especially important when using polarization as the size of the particles must be small enough to follow the flow and to maintain the polarization of the incident light upon scattering. In our tests the seed material for the jet flow was 0.5µm alumina powder dispersed in the flow well upstream of the nozzle using an air-assisted atomizing nozzle to atomize ethanol carrying the particles. The ambient fluid was seeded with 0.2µm oil droplets produced by a commercial 'smoke' generator. We made several iterations on ambient seeding arrangements, finally settling on a method of releasing oil droplet 'smoke' from a commercial fogger that essentially replicated a very low velocity freejet around the research jet. With this set of seeders we achieved seeding adequate for good velocity vector determination at each point in the map over 90% of the time.

Finally it should be noted that given the optical setup and the particle size the cameras were not actually imaging the particles. This is a good thing because the particles images would have been less than a pixel in size, leading to a problem with peak locking in the image correlation processing. The effect of ‘defocusing’ the image system was to allow the particle image to cover more than a pixel, assuring the correlation algorithm of finding a parabolic peak in the correlation domain from which a subpixel peak could be determined.

Space-Time Data Acquisition Strategy

A priori determination of the proper space and time displacements at which to make measurements so as to capture the peak correlation as the turbulence advects and decays was important. Estimates of the local Strouhal number, average convection speed, and the temporal decay rate in the Lagrangian frame guided the proper combinations of displacement in time and space to capture the peak correlation. Given the need to economize on the number of discrete time delays over which data was acquired, an exponentially increasing set of six time delays was determined which best captured the expected Gaussian decay. Corresponding spatial separations were then computed to move the two systems apart about the reference location so as to capture the same flow structures at the two different times.

Datasets were acquired about five different axial reference locations in the $D = 51\text{mm}$ jet: $x_1/D = 2, 6, 10, 16,$ and 22 for seven different flow conditions as given in Table 1. The flow conditions were chosen from a larger matrix of conditions being used to build up a jet aero/acoustic database and contain essentially three different velocities and temperature ratios using different combinations of pressure ratio and temperature ratio. Given the displacements used around each reference point the jet plume was fully covered by multiple datasets which could be averaged to provide measurements of single-point statistics such as mean and variances of velocity.

Table 1 Definition of test conditions.

Set point	M_j	T_j/T_∞	NPR	M
3	0.500	0.950	1.197	0.513
7	0.900	0.835	1.861	0.985
23	0.500	1.764	1.102	0.376
27	0.900	1.764	1.357	0.678
29	1.330	1.764	1.888	1.001
46	0.900	2.700	1.219	0.548
49	1.485	2.700	1.678	0.904

RESULTS AND DISCUSSION

Note About Data Quality

In PIV work, the time averages are computed as ensemble averages over uncorrelated instantaneous captures of velocity fields. In processing the images to velocity maps several criteria are used to determine if an instantaneous velocity vector is valid and to remove those vectors that are ‘obviously bad’. Generally speaking, the more points have to be thrown out, the more suspect the data is. An important statistic for diagnostic purposes is the data quality, defined as the number of accepted vectors at a point relative to the total number of vector maps acquired. For the data used in computing the single and two-point statistics presented here there are only a few regions, mostly near edges of the individual images that make up the composite, where the quality is below 0.95. This usually alerts us that statistics in these regions may be corrupted by bad points and makes the data have less significance in analysis. In computing composite maps, statistics from the various overlapping regions were combined, weighted by the data quality to reduce the error in the composite statistic.

Another issue that can plague PIV measurements is peak locking, a phenomena where subpixel determination of correlation peaks is defeated by having images where the particle images do not cover more than a single pixel on the camera. This is a very real problem with large fields of view such as are needed in computing spatial correlations. This problem can be checked by looking for peaks corresponding to integer pixel displacements in the histogram of velocities over an image and slightly defocusing the image if needed.

Single-Point Statistics

Comparisons with historical data

Figure 3 shows the distribution of mean axial centerline velocity at all measured conditions. On the left is the data plotted in physical axial coordinates, while on the right is the same data plotted against the correlation parameter given by Witze¹⁶. The correlation does a find job collapsing all the data and showing that the acquired data is at least good to the level of mean velocity. One of the data sets, that of setpoint 46 seems to show some problems downstream of 10 diameters; no explanation has been found so far for this behavior. Ahuja et al.⁹ published mean and rms centerline data for jets with similar conditions to setpoints 7 and 46. The present results are overlaid in Figure 4. The mean velocities agree very well aside from the issues noted above with setpoint 46 data. The rms values are a bit high for the PIV data, especially downstream of the peak in the cold jet case.

Two-dimensional fields

Figure 5 shows the distribution of axial velocity for setpoints 7 and 46, highlighting the effect of temperature on a $M_j = 0.9$ jet. The reduction in the potential core with temperature is very dramatic as is the general foreshortening of the plume. Figure 6, showing the turbulent kinetic energy (TKE) for the same two cases, shows the dramatic increase in turbulence that accompanies the shortened potential core. Just from simple ideas of how sound source strength is related to turbulent kinetic energy one would expect that the hot jet might produce more noise in the first few jet diameters. Of course, one would have to convert the TKE to acoustic energy at the rough rate of $TKE^{7/2}$ and integrate over the volume before making even a simple statement about relative noise production. Finally, Figure 7 gives more detail about the turbulent kinetic energy, showing the ratio of radial and axial variances, or turbulence isotropy. Given that turbulence isotropy is a characteristic which theory says can change the efficiency of the noise produced by turbulence it seems that the hot jet, having less isotropy, should be more efficient a noise generator as well. One very interesting detail that seems valid is the low value of turbulence isotropy along the peak of the TKE surrounding the potential core. Another observation: the turbulence never reaches isotropy, or ratio unity even 25 or more diameters downstream. Both of the observations were found in all the cases studied.

Two-Point Statistics

Space-Time Statistics

It is rather difficult to present the space-time correlation data in a fashion that suits all needs for theoretists interested in the data. At some point the data will be available for electronic distribution via NASA's dissemination sites. For this paper we will only look in-depth at the correlation of axial velocity at a reference location of $x_1/D=10$, $x_2/D=0.5$ in the $M_j=0.9$, $T_j/T_\infty = 0.86$ (setpoint 7) jet. Similar data was acquired for the other six setpoints and with analysis at $x_1/D = 2, 6, 16$, and 22, and at $-1 < x_2/D < 1$. In the end we will present the integral quantities (length and timescales) which summarize the data and are most useful for turbulence modeling for jet noise.

For orientation we present the correlation of axial velocity $R_{11}(\xi, \tau)$ in slices, first in planes of constant time delay corresponding to the time delays measured, then in planes of constant $\xi_1 - U_c \tau = 0$ and $\xi_2 = 0$ (Figure 8). The correlations at a given time slice have roughly elliptic contours at most levels centered on $\xi_2 = 0$ and an axial displacement corresponding to a near-constant convection velocity. Only at the last time instance does the advection speed seem to change, and by then picking a peak is rather difficult.

In a slice through the data at $\xi_2 = 0$ we clearly see the decay of the correlation, the peak decreasing and the width increasing with time. This being the correlation of axial velocity with axial displacement, the correlation is not expected to go negative by reasoning of grid turbulence; however, there is significant negative correlation presumably due to the influence of large scale structures. If one considers the correlation to represent a turbulent structure, the negative correlations upstream and downstream represent other structures that are correlated in a negative sense. The fact that these negative regions do not decay as strongly as the positive regions is another indicator that these are long-time coherent, large structures which may impact the low frequency sound sources represented by this correlation.

In the slice through the data following the peak correlation location, $\xi_1 - U_c \tau = 0$, we see the correlation of axial velocity with radial direction. Here, homogeneous turbulence theory expects significant negative correlation, and these do exist and they decay at much the same rate as the positive regions.

In an ideal world, the correlation coefficient would be exactly unity at zero separation in space and time. However, it is impossible for two systems, in this case two PIV systems, to measure exactly the same value, hence the correlation value will not be unity. In fact, the correlation was significantly less than one, usually between 0.8 and 0.9. As seen in Figure 9, where R_{11} computed from cross-correlation is compared with the R_{11} computed from autocorrelation, the error in the cross-correlation is limited to very near the peak of the correlation. Some part of this seems due to slight differences in registration of the two imaging systems, an error that can be simulated by displacing a second copy of the velocity fields in a direction normal to that over which the correlation is being computed. As seen in Figure 9, the error introduced by this artificial misregistration is similar to that found in the cross-correlation data.

Next we isolate the spatial correlations in the axial ($R_{11}(\xi_1, \xi_2=0, \tau=0)$) and radial ($R_{11}(\xi_1=0, \xi_2, \tau=0)$) directions at zero time delay. Three radial locations are shown in Figure 10: $x_2/D = -0.5, 0.0, +0.5$, all at $x_1/D = 10$. Noteworthy here is the strong negative correlations at $\xi_1 = \pm 1$ obtained for $x_2/D = 0.0$. Thinking in terms of jet structures instead of homogeneous turbulence, having velocities in the two shear layers negatively correlated indicates a strong asymmetric mode to the unsteady flow at the end of the potential core. While this is not surprising, it does explain why the radial lengthscale tends to be small right on the centerline of the jet, as will be seen later.

For temporal correlation, we track the peak of $R_{11}(\xi_1, \xi_2=0, \tau_i)$ for the six different time delays τ_i as

shown in Figure 10. From the peaks of these correlations we can obtain the decay in axial correlation in Lagrangian frame. Picking out the peaks is a tricky business and a great deal of effort has gone into developing algorithms that can reliably pick out peaks from noisy data with different lengthscales. Using an iterative method, the lengthscales of the spatial correlations at each time delay are estimated and used as a moving average window to smooth the data and identify the best peak. Near zero time delay the window is usually only a few cells wide, while at large time delays the window becomes rather large.

Integral Measures

From the two-point space-time correlations, such as were presented in depth above, length and timescales have been computed for all the flows on a spatial grid of the five different axial locations and nine radial locations. Figure 11 presents the axial lengthscale L_{11} for the setpoints 7 and 46 corresponding to the cases shown in figures Figure 5-Figure 7. Note the logarithmic scale for the lengthscales. Also note the superimposed mesh, showing the actual locations where the lengthscale measurements were actually made.

Axial lengthscales vary only by 50% across the jet at any given axial location, and vary from $0.08D$ at $x_1/D = 2$ to nearly 1 at $x_1/D = 22$. In a similar fashion integral lengthscales L_{12} , L_{21} , and L_{22} have also computed.

Unlike axial lengthscales, there is a significant difference in integral timescales between the cold and hot jets, as shown in Figure 12. Again, note the logarithmic scales of the plot. Timescales computed from axial velocity vary from $0.02U_j/D$ at $x_1/D = 2$ to nearly 10 at $x_1/D = 22$ and differ by a factor of 2 between hot and cold jets.

Approximation of fourth order correlations by products of second order correlations.

In many aeroacoustic prediction schemes the required fourth-order correlation of velocity is approximated by a product of second-order correlations under the assumption of normal joint probability distributions of the velocity:

$$I_{ijkl} = \overline{u_i u_j u_k' u_l'}$$

$$\approx \overline{u_i u_j} \overline{u_k' u_l'} + \overline{u_i u_k'} \overline{u_j u_l'} + \overline{u_i u_l'} \overline{u_j u_k'} \equiv R_{ij} R_{kl}$$

This assumption was evaluated using the PIV data even though the high order of the statistics causes the measurements to have rather large uncertainties. Figure 13 compares the axial and radial components of the fourth order correlation, I_{1111} and I_{2222} , with their second order approximations, $R_{11}R_{11}$ and $R_{22}R_{22}$ for planes of $(\xi_1, \xi_2 = 0, \tau)$ at $x_1/D=10, x_2/D=0.5$ in the $M_j=0.9, T_j/T_\infty = 0.86$ jet. There is considerably more scatter in the I_{1111} measures and I_{2222} is perhaps a bit stronger than $R_{22}R_{22}$.

These were the two trends most notable in spot checks of these statistics at other jet conditions and other locations. Overall, however, the two statistics agreed within the 10% or so error band that seemed to characterize the measurements.

CONCLUSIONS

Clearly the main conclusion of the work presented in this paper is that turbulence statistics, up to and including two-point space-time velocity correlations, can be obtained in hot, high-speed jets using PIV. Comparisons with previous data for low order statistics show that PIV runs into problems when the spatial resolution is too low, such as in the near-jet region where we did not allow more than a few velocity measurements across the shear layer. It also shows the importance of obtaining good particle images as erroneously high turbulence levels seem to accompany regions of low confidence velocity determinations.

From the limited analysis conducted on the data to date, we can see the strong impact of heat on the jet potential core and the turbulent kinetic energy. We also see the slight impact on turbulence isotropy and the correlation of low isotropy with regions of strong turbulence in the shear layer surrounding the potential core. We find the interesting result that heat does not strongly change the axial lengthscales even though it does change the timescales. Finally we note that the second order approximations to the fourth order correlations needed for jet noise theory are nearly within the uncertainty in computing these quantities in the jet.

REFERENCES

- ¹ Seiner, J.M., Ukeiley, L.S., Ponton, M.K., and Jansen, B.J., 2002 "Progress in experimental measure of turbulent flow for aeroacoustics," *AIAA 2002-2402*.
- ² Lighthill, M.J. 1952, "On sound generated aerodynamically, I. General theory," *Proc. Royal Soc. London A*, **211**, 564-587.
- ³ Lilley, G.M., Morris, P.J., & Tester, B.J., 1973, "On the theory of jet noise and its applications," *AIAA Paper* 73-987.
- ⁴ Batchelor, G.K, 1953, *The Theory of Homogeneous Turbulence*, Cambridge University Press.
- ⁵ Chu, W.T.1966, "Turbulence measurements relevant to jet noise," *Univ. Toronto Institute for Aerospace Studies UTIAS Report* 119.
- ⁶ Laurence, J.R. 1956, "Intensity, scale, and spectra of turbulence in mixing region of free subsonic jet," *NACA Report* 1292.

⁷ Davies, P.O.A.L., Fisher, K.J., and Barratt, M.J. 1963, "The characteristics of turbulence in the mixing region of a round jet," *J Fluid Mech* **15**, 337-367.

⁸ Bradshaw, P., Ferriss, D.H., Johnson, R.F. 1963, "Turbulence in the noise-producing region of a circular jet," *J Fluid Mech* **19**, 591-625.

⁹ Ahuja, K.K., Lepicovsky, J., Tam, C.K.W., Morris, P.J., and Burrin, R.H. 1982 "Tone-excited jet: Theory and experiments," NASA CR-3538.

¹⁰ Oakley, T.R., Loth, E., Adrian, R.J., 1996, "Cinematic particle image velocimetry of high-Reynolds-number turbulent free-shear layer," *AIAAJ* **34**(2), 299-308.

¹¹ Hu, H. Saga, T., Kobayashi, T. and Taniguchi, N., 2002, "Simultaneous measurements of all three

components of velocity and vorticity vectors in a lobed jet flow by means of dual-plane stereoscopic particle image velocimetry," *Phys Fluids* **14** (7), 2128-2138.

¹² Khavaran, A. 1999, "On the role of anisotropy in turbulent mixing noise," *AIAAJ* **37**.

¹³ Hunter, C.A. 2002, *An Approximate Jet Noise Prediction Method Based on Reynolds-Averaged Navier-Stokes Computational Fluid Dynamics Simulation*, PhD dissertation, George Washington University.

¹⁴ Tam, C.K.W. & Auriault, L. 1999, "Jet mixing noise from fine-scale turbulence," *AIAAJ* **37**, 145-153.

¹⁵ Hunter, C.A. 2002, PhD Dissertation Addendum.

¹⁶ Witze, P.O., 1974, "Centerline velocity decay of compressible free jets," *AIAA J* **12**(4), 417-418.

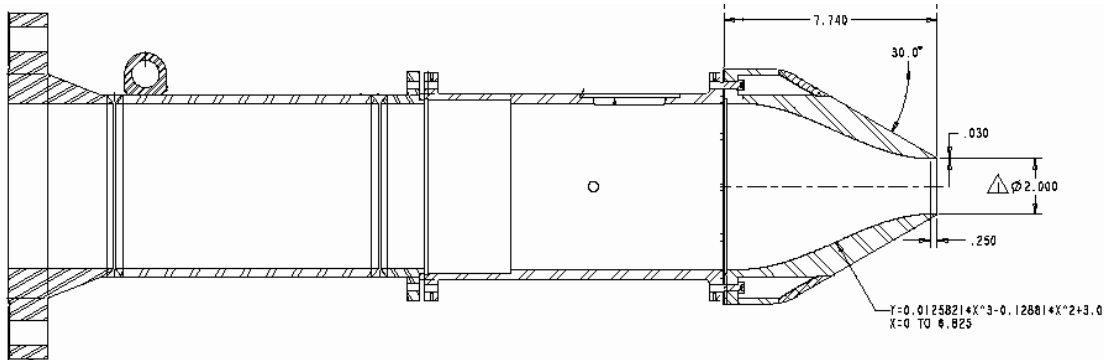


Figure 1.—NASA Acoustic Reference Nozzle system, with ARN2 (51mm diameter) nozzle.

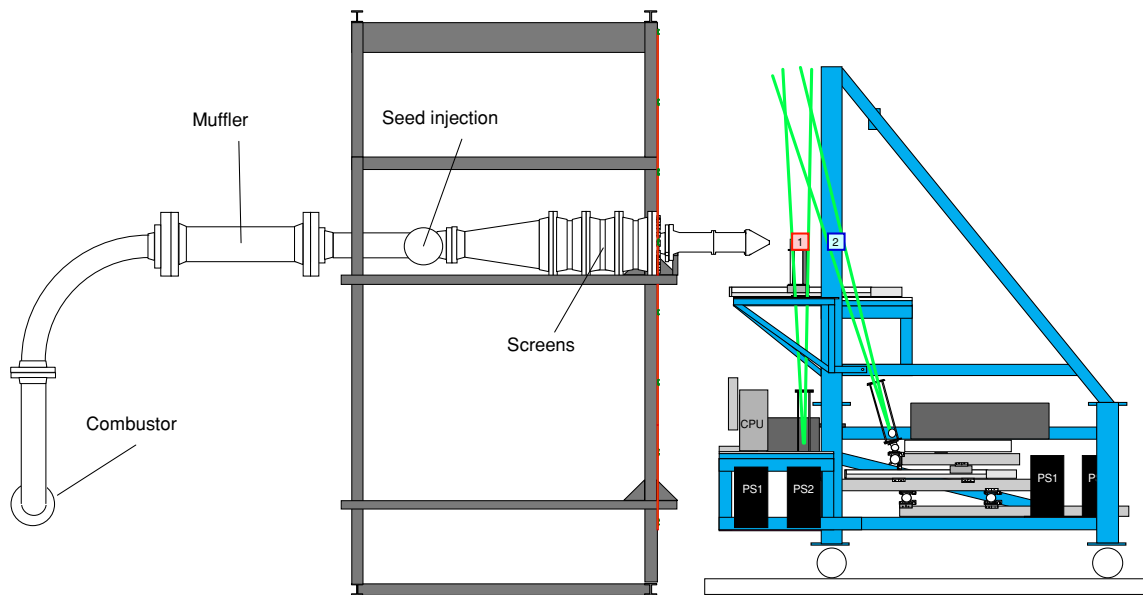


Figure 2.—SHJAR with Dual PIV setup.

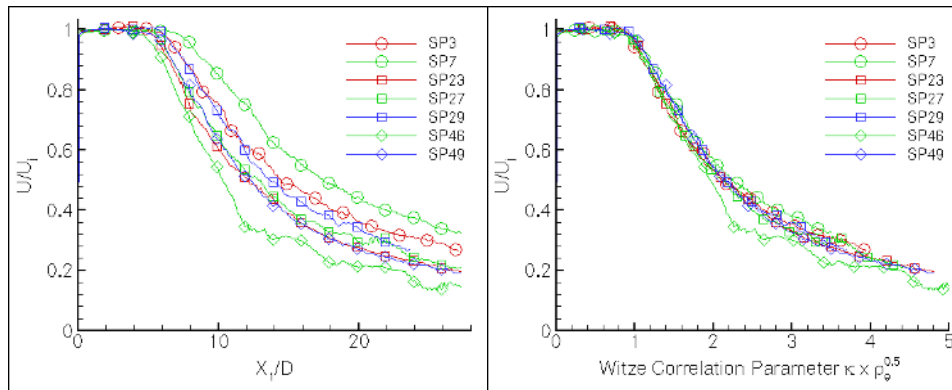


Figure 3.—Measured centerline decay of mean axial velocity for all measured conditions: as measured (left) and collapsed using Witze correlation parameter (right).

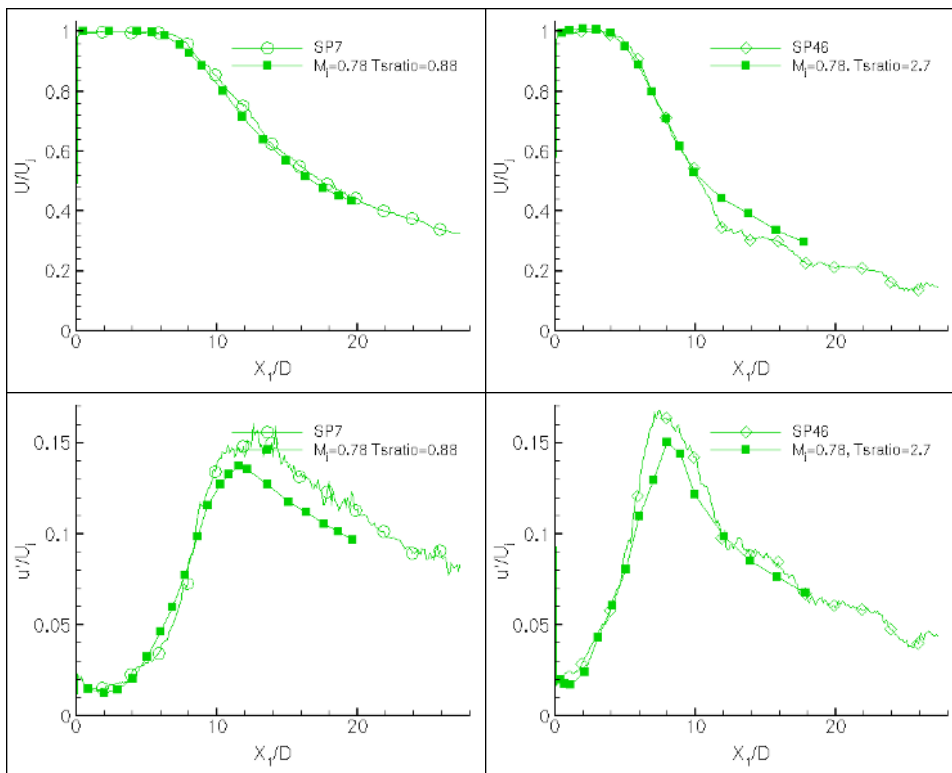


Figure 4.—Comparison of PIV results with that of LDV [9] for $M_j=0.9$, $T_j/T_\infty = 0.86$ (left) and $T_j/T_\infty = 2.7$ (right) on jet centerline. Top: U_1/U_j , Bottom: u_1^2/U_j^2 .

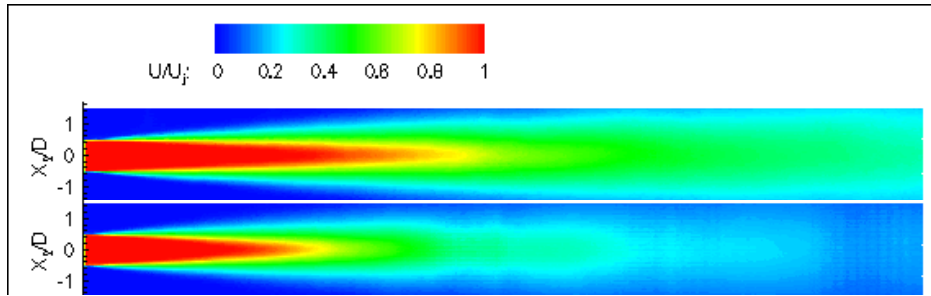


Figure 5.—Mean velocity fields, $M_j=0.9$, $T_j/T_\infty = 0.86$ (top) and $T_j/T_\infty = 2.7$ (bottom).

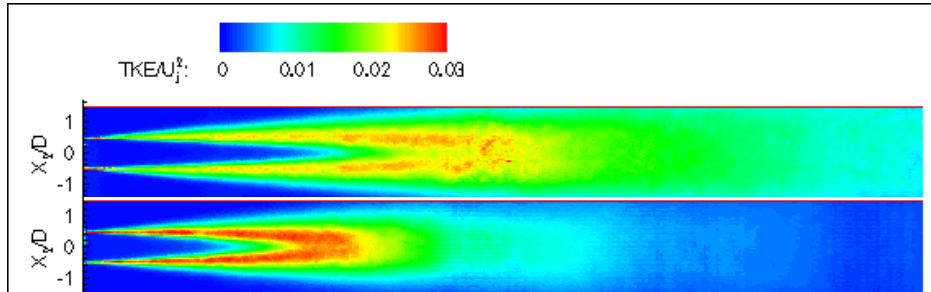


Figure 6.—Turbulent kinetic energy. $M_j=0.9$, $T_j/T_\infty = 0.86$ (top) and $T_j/T_\infty = 2.7$ (bottom).

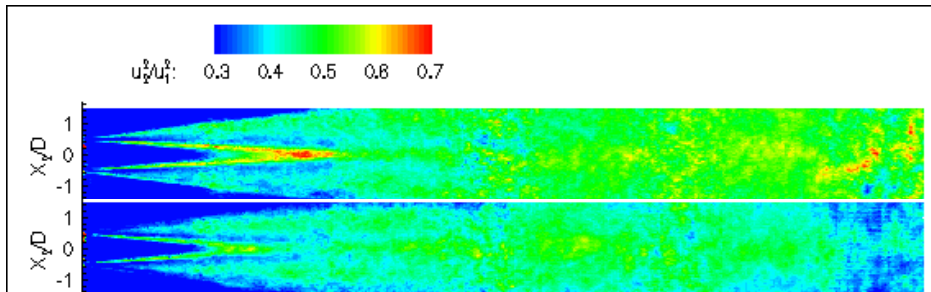


Figure 7.—Turbulence anisotropy, $M_j=0.9$, $T_j/T_\infty = 0.86$ (top) and $T_j/T_\infty = 2.7$ (bottom).

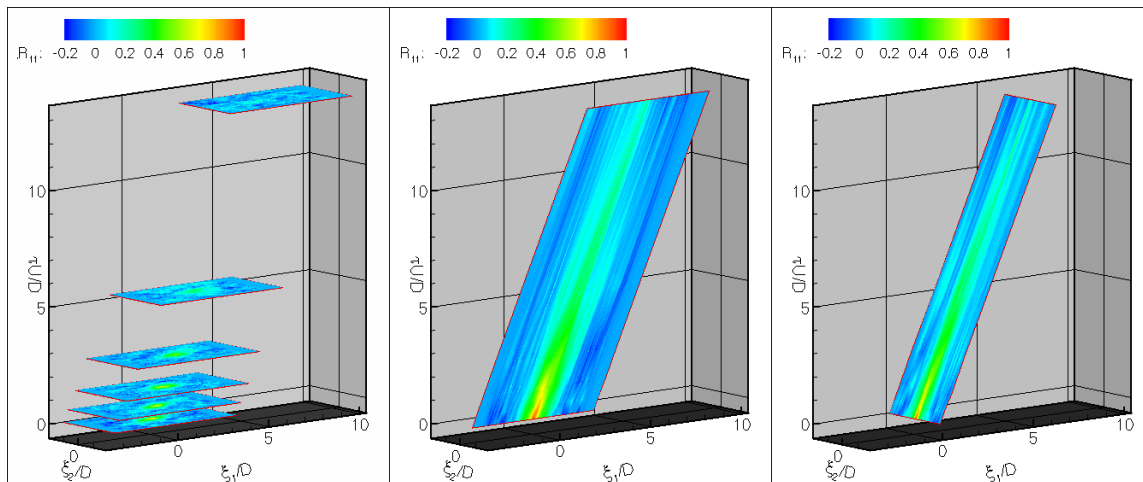


Figure 8.—Space-time correlation $R_{11}(\xi, \tau)$ at $x_1/D=10, x_2/D=0.5$ in $M_j=0.9$, $T_j/T_\infty = 0.86$ jet. Sections cut at constant τ (left), $\xi_2 = 0$ (middle), and $\xi_1 - U_c \tau = 0$ (right).

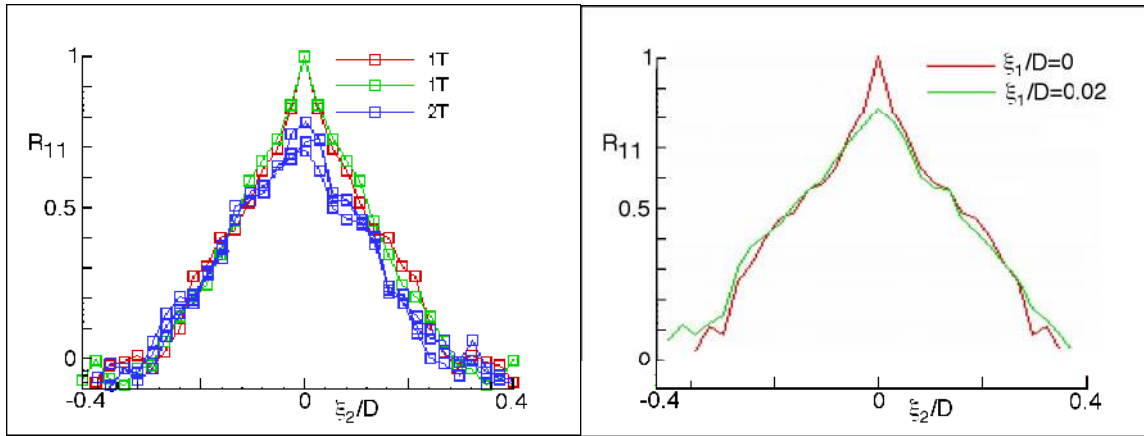


Figure 9.—Comparison of spatial correlation computed via autocorrelation from two PIV datasets and via cross-correlation of the two PIV datasets (left). Comparison of autocorrelation normally and with shift, simulating misregistration of two systems (right).

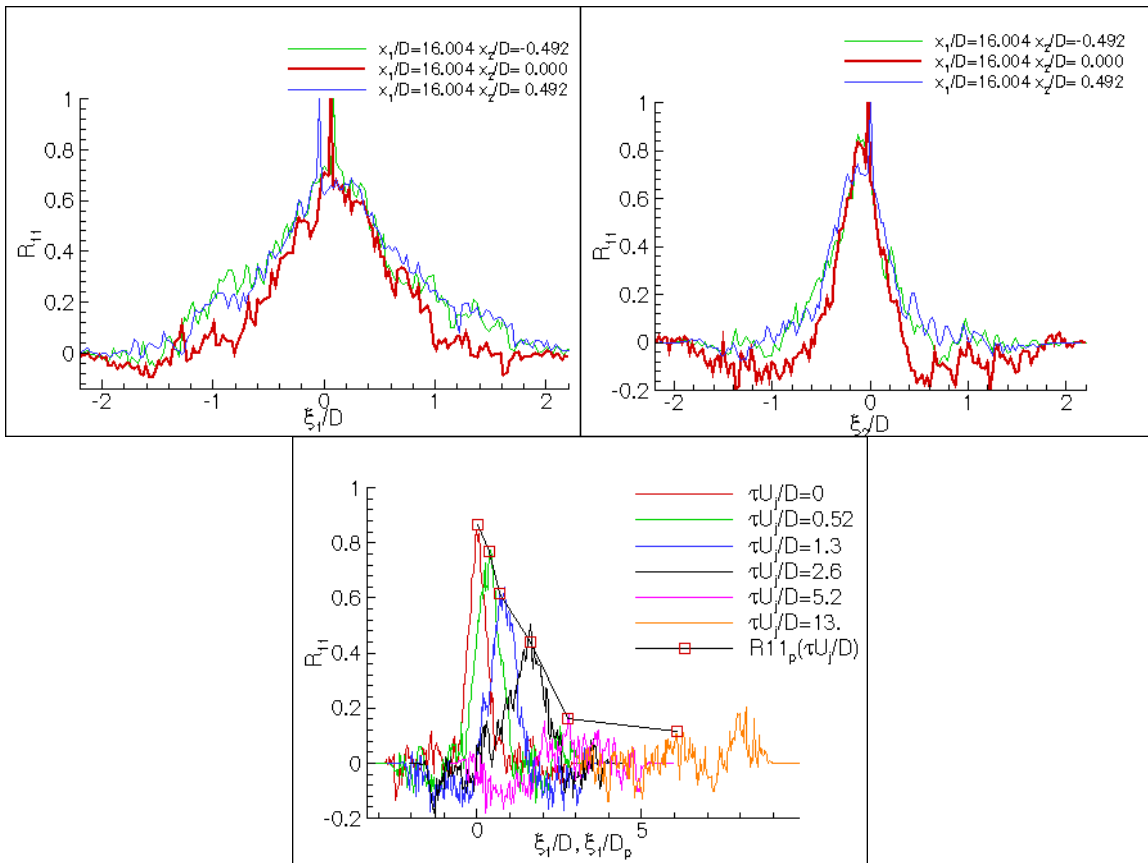


Figure 10.—Spatial correlation of axial velocity in ξ_1 (top left) and ξ_2 (top right) at zero time delay for various radial locations, and in ξ_1 at various time delays showing the decay of the peak correlation (bottom). Reference point is $x/D=10$ in $M_j=0.9$, $T_j/T_\infty = 0.86$ jet.

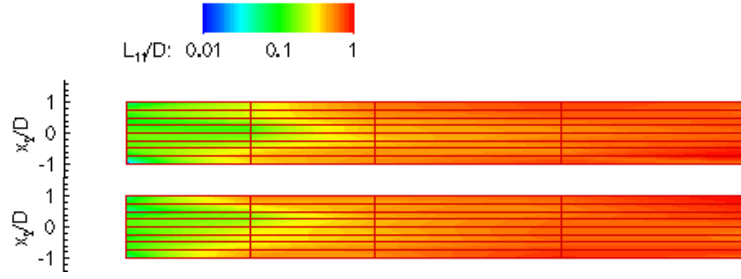


Figure 11.—Axial lengthscale L_{11} , for $M_j=0.9$, $T_j/T_\infty = 0.86$ (top) and $T_j/T_\infty = 2.7$ (bottom).

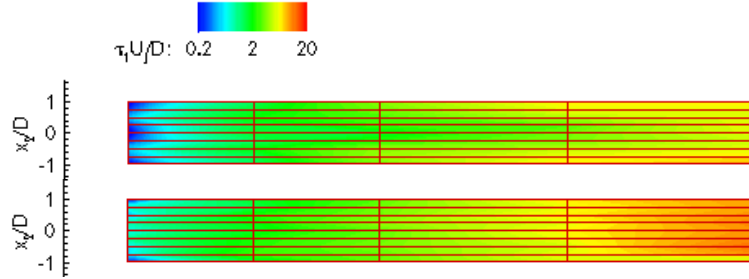


Figure 12.—Integral timescales of the axial velocity for $M_j=0.9$, $T_j/T_\infty = 0.86$ (top) and $T_j/T_\infty = 2.7$ (bottom).

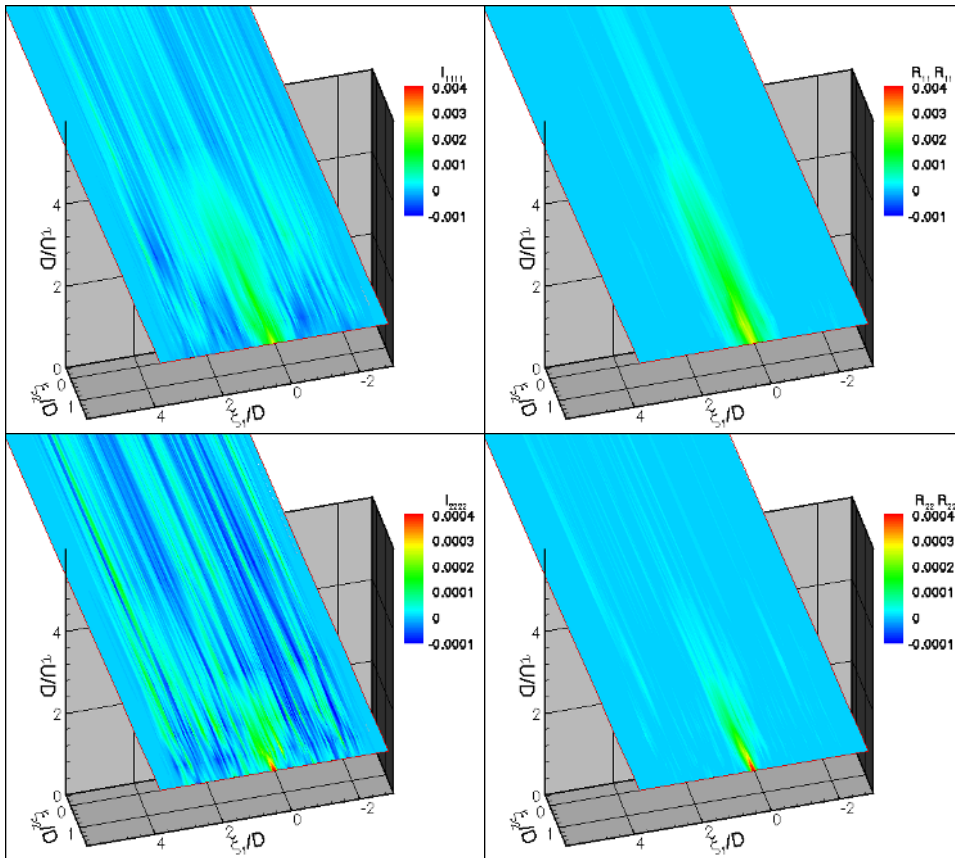


Figure 13.—Comparisons of 4th order correlations (left) with 2nd order approximations (right) based upon assumption of normal probability distribution. I_{1111} and $R_{11}R_{11}$ (top) and I_{2222} and $R_{22}R_{22}$ (bottom) as functions of axial displacement ξ_1 and time delay τ at $x_1/D=10, x_2/D=0.5$ in $M_j=0.9$, $T_j/T_\infty = 0.86$ jet.

REPORT DOCUMENTATION PAGEForm Approved
OMB No. 0704-0188

Public reporting burden for this collection of information is estimated to average 1 hour per response, including the time for reviewing instructions, searching existing data sources, gathering and maintaining the data needed, and completing and reviewing the collection of information. Send comments regarding this burden estimate or any other aspect of this collection of information, including suggestions for reducing this burden, to Washington Headquarters Services, Directorate for Information Operations and Reports, 1215 Jefferson Davis Highway, Suite 1204, Arlington, VA 22202-4302, and to the Office of Management and Budget, Paperwork Reduction Project (0704-0188), Washington, DC 20503.

1. AGENCY USE ONLY (Leave blank)		2. REPORT DATE February 2004	3. REPORT TYPE AND DATES COVERED Technical Memorandum	
4. TITLE AND SUBTITLE Measurements of the Aeroacoustic Sound Source in Hot Jets			5. FUNDING NUMBERS WBS-22-781-30-27	
6. AUTHOR(S) James Bridges and Mark Wernet				
7. PERFORMING ORGANIZATION NAME(S) AND ADDRESS(ES) National Aeronautics and Space Administration John H. Glenn Research Center at Lewis Field Cleveland, Ohio 44135-3191			8. PERFORMING ORGANIZATION REPORT NUMBER E-14068	
9. SPONSORING/MONITORING AGENCY NAME(S) AND ADDRESS(ES) National Aeronautics and Space Administration Washington, DC 20546-0001			10. SPONSORING/MONITORING AGENCY REPORT NUMBER NASA TM-2004-212508 AIAA-2003-3130	
11. SUPPLEMENTARY NOTES Prepared for the Ninth Aeroacoustics Conference and Exhibit cosponsored by the American Institute of Aeronautics and Astronautics and the Confederation of European Aerospace Societies, Hilton Head, South Carolina, May 12-14, 2003. Responsible person, James Bridges, organization code 5940, 216-433-2693.				
12a. DISTRIBUTION/AVAILABILITY STATEMENT Unclassified - Unlimited Subject Categories: 02 and 34 Available electronically at http://gltrs.grc.nasa.gov This publication is available from the NASA Center for AeroSpace Information, 301-621-0390.			12b. DISTRIBUTION CODE	
13. ABSTRACT (Maximum 200 words) We have succeeded in measuring a substantial portion of the two-point space-time velocity correlation in hot, high-speed turbulent jets. This measurement, crucial in aeroacoustic theory and the prediction of jet noise, has been sought for a long time, but has not been made due to the limitations of anemometry. Particle Image Velocimetry has reached a stage of maturity where sufficient measurement density in both time and space allow the computation of space-time correlations. This paper documents these measurements along with lower-order statistics to document the adherence of the jet rig and instrumentation to conventional measures of the turbulence of jets. These measures have been made for a simple round convergent nozzle at acoustic Mach numbers of 0.5, 0.9, both cold and at a static temperature ratio of 2.7, allowing some estimation of the changes in turbulence that take place with changes in jet temperature. Since the dataset described in this paper is very extensive, attention will be focused on validation of the rig and of the measurement systems, and on some of the interesting observations made from studying the statistics, especially as they relate to jet noise. Of note is the effort to study the acoustically relevant part of the space-time correlation by addressing that part of the turbulence kinetic energy that has sonic phase speed.				
14. SUBJECT TERMS Turbulence models; Velocity distribution; Turbulence; Jet flow; Supersonic speed; Nozzle flow; High speed; Jet aircraft noise; Aerodynamic noise; Aeroacoustics; Correlation; Particle image velocimetry			15. NUMBER OF PAGES 17	
			16. PRICE CODE	
17. SECURITY CLASSIFICATION OF REPORT Unclassified	18. SECURITY CLASSIFICATION OF THIS PAGE Unclassified	19. SECURITY CLASSIFICATION OF ABSTRACT Unclassified	20. LIMITATION OF ABSTRACT	